Clim Dyn
DOI 10.1007/s00382-017-3624-y

Prolonged effect of the stratospheric pathway in linking Barents–Kara Sea sea ice variability to the midlatitude circulation in a simplified model

Pengfei Zhang[1] · **Yutian Wu**[1] · **Karen L. Smith**[2]

Received: 16 November 2016 / Accepted: 6 March 2017

Abstract To better understand the dynamical mechanism that accounts for the observed lead-lag correlation between the early winter Barents–Kara Sea (BKS) sea ice variability and the later winter midlatitude circulation response, a series of experiments are conducted using a simplified atmospheric general circulation model with a prescribed idealized near-surface heating over the BKS. A prolonged effect is found in the idealized experiments following the near-surface heating and can be explicitly attributed to the stratospheric pathway and the long time scale in the stratosphere. The analysis of the Eliassen-Palm flux shows that, as a result of the imposed heating and linear constructive interference, anomalous upward propagating planetary-scale waves are excited and weaken the stratospheric polar vortex. This stratospheric response persists for approximately 1–2 months accompanied by downward migration to the troposphere and the surface. This downward migration largely amplifies and extends the low-level jet deceleration in the midlatitudes and cold air advection over central Asia. The idealized model experiments also suggest that the BKS region is the most effective in affecting the midlatitude circulation than other regions over the Arctic.

Keywords Stratosphere–troposphere coupling · Nudging method · Planetary-scale wave propagation · Barents–Kara Sea sea ice · Midlatitude low-level jet · Cold advection over central Asia

1 Introduction

Previous studies have found that Arctic sea ice variability and the resulting temperature perturbation, especially over the Barents–Kara Sea (BKS), can strongly affect the Northern Hemisphere (NH) midlatitude circulation, such as the westerly jet and planetary-scale waves, and possibly blocking frequency and Eurasian cold spells (e.g., Honda et al. 2009; Francis and Vavrus 2012; Cohen et al. 2014; Mori et al. 2014; Vihma 2014; Barnes and Screen 2015; Hassanzadeh and Kuang 2015; Kug et al. 2015; Lee et al. 2015; Screen et al. 2015). From observations, sea ice variability over the entire Arctic has been found to precede the anomalous wintertime tropospheric circulation by about 2–4 months (Wu and Zhang 2010). Over the BKS region, the sea ice variability maximizes in autumn (not shown), with November (Nov) sea ice exerting the largest impact on the midlatitude circulation in the subsequent winter (Koenigk et al. 2016; Yang et al. 2016). Figure 1a shows the regression of surface air temperature (SAT) on the Nov BKS sea ice concentration (SIC) after removing the long-term trend and the El Niño-Southern Oscillation (ENSO) related component (data and calculation details can be found in Sect. 2). Significant anomalous warm SAT associated with lower than normal BKS SIC can be seen in Nov and December (Dec) over the BKS region. The maximum SAT difference is about 9 K between low and high Nov BKS SIC index years (defined by exceeding ±0.8 standard deviation). The response of the NH midlatitude jet stream,

Electronic supplementary material The online version of this article (doi:10.1007/s00382-017-3624-y) contains supplementary material, which is available to authorized users.

✉ Pengfei Zhang
zpengfei@purdue.edu

[1] Department of Earth, Atmospheric and Planetary Sciences, Purdue University, West Lafayette, IN, USA

[2] Lamont-Doherty Earth Observatory, Columbia University, Palisades, NY, USA

Published online: 11 April 2017

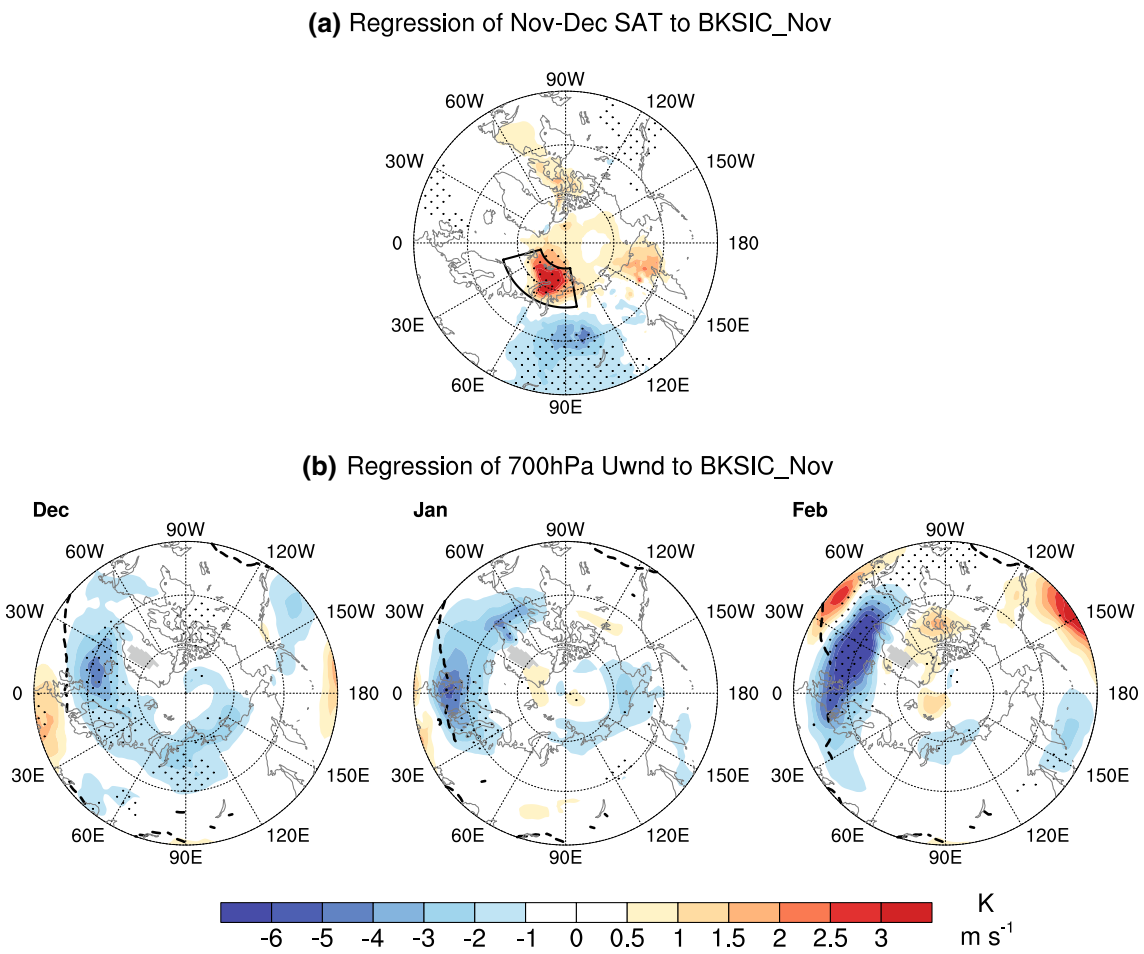

Fig. 1 Regression of surface air temperature (SAT, units: K) in November and December on the normalized November BKS SIC (**a**). **b** is the same as **a** but for 700 hPa zonal wind (*color shading*, units: m s^{-1}) in December, January and February. Stippling denotes the 95% confidence level. The *black curves* in **a** mark the BKS region. The *dashed lines* in **b** denote the climatological position of westerly jet. The sign of SIC is reversed here to emphasize the impact of lower than normal SIC on SAT and zonal wind. The data information and calculation method can be found in Sect. 2

however, is not synchronized with the SAT anomaly but rather is maximized over the North Atlantic-Europe sector during January (Jan) and February (Feb) (Fig. 1b), which is about 2–3 months after the Nov BKS SIC variability and about 1–2 months after the SAT perturbation. However, the dynamical mechanism that accounts for this lead-lag relationship has not yet been fully explored.

Stratospheric processes, whose time scales are longer than that of the troposphere (e.g., Baldwin et al. 2003), may provide a possible explanation. Recent studies have suggested an important role of the stratospheric pathway in linking the Arctic with the midlatitude circulation via upward wave propagation and downward migration (Sun et al. 2015; Nakamura et al. 2016; Wu and Smith 2016). The enhanced upward propagating planetary-scale waves due to sea ice loss could penetrate into the stratosphere, increase the geopotential height and decelerate the westerly in the stratosphere, and thus weaken the stratospheric polar vortex (Jaiser et al. 2013; Kim et al. 2014). These stratospheric circulation responses are likely to persist in the stratosphere for a couple of months accompanied by downward migration back to the troposphere and the surface (Kim et al. 2014; Sun et al. 2015; Nakamura et al. 2016). This is in addition to the tropospheric pathway that involves transient eddy adjustment to change in meridional temperature gradient (Deser et al. 2004). Previous studies (Sun et al. 2015; Nakamura et al. 2016; Wu and Smith 2016) have suggested that the stratospheric pathway could be as important as the tropospheric pathway in influencing the midlatitude circulation; however, no previous work, to the best of our knowledge, has explicitly quantified the role of the stratospheric pathway in linking the early winter sea ice variability with the later winter midlatitude circulation.

In this study we aim to address the following questions: What is responsible for the 1–2 months lag between the BKS temperature perturbation and NH midlatitude

circulation response? And what is the underlying dynamical mechanism? We hypothesize that the prolonged effect is a result of the stratospheric pathway and we use an idealized AGCM and apply a nudging method in the model to explicitly test this hypothesis.

The paper is organized as follows. Section 2 describes the observational datasets, model setup, and design of the numerical experiments. Section 3 discusses the results from the idealized model experiments including the prolonged effect of the stratospheric pathway and the associated dynamical mechanisms, induced cold winter over the central Asia and the sensitivity to the forcing location. The paper concludes with a summary and discussion in Sect. 4.

2 Data and model simulations

2.1 Observation datasets and statistical significance

The European Centre for Medium-Range Weather Forecasts (ECMWF) reanalysis ERA-Interim is used to represent the atmospheric circulation in Fig. 1, whose horizontal resolution is 1.5°longitude × 1.5°latitude with 37 vertical levels (Dee et al. 2011). The sea ice concentration (SIC) dataset is 25km × 25 km high-resolution data derived from passive microwave satellite data with the National Aeronautics and Space Administration (NASA) team algorithm (Cavalieri et al. 1996). The sea surface temperature (SST) dataset used to calculate the Niño 3.4 index is from the National Oceanic and Atmospheric Administration (NOAA) Optimum Interpolation (OI) SST Version 2 on a 1°longitude × 1°latitude resolution (Reynolds et al. 2002). Monthly variables during 1982–2014 are used in Fig. 1.

We define the Nov BKS SIC index using the area-averaged SIC in the region of 15°–100°E and 70°–82°N as highlighted by the black curves in Fig. 1a. Here we reverse the sign of SIC to emphasize the effect associated with lower than normal SIC. For all the fields in Fig. 1, both the long-term trend and the ENSO related component (calculated as the linear regression on Niño 3.4 index) are removed to focus on year-to-year variability.

In addition, statistical significance test in this study is two samples two tails student *t* test except Figs. 3d and 8e, f which are one sample *t* test.

2.2 Model, forcing and experimental design

The idealized AGCM used in this study is the dry dynamical core, developed at the Geophysical Fluid Dynamics Laboratory (GFDL). The model is based on the primitive equations and idealized physics, and the temperature equation is driven by a Newtonian relaxation toward a zonally symmetric equilibrium temperature profile (Held and Suarez 1994). A simple representation of the stratospheric polar vortex and an idealized seasonal cycle in both the troposphere and stratosphere are included following Polvani and Kushner (2002) and Kushner and Polvani (2006). Realistic topography is also used in the model to excite a rather realistic planetary-scale stationary wave pattern (Smith et al. 2010). In general, the simulated zonal wave-1 and wave-2 stationary wave pattern compares well with observations except for a weaker magnitude (Figure S1). In addition, the ridge/trough center of simulated wave-1 compares well with observations in the lower troposphere (not shown) but shifts slightly to the east (by about 30° longitude) at 300 hPa (Figure S1). We integrate the model at a horizontal resolution of T42 with 40 vertical levels in sigma coordinate.

In addition to the control run (CTRL), a series of perturbation experiments are performed (Table 1). Following the approach in previous studies (e.g., Butler et al. 2010; Smith et al. 2010; Wu and Smith 2016), in the perturbation experiments, an additional heating profile, ΔQ, is added to the temperature tendency equation: $\frac{\partial T}{\partial t} = \ldots \kappa_T \left[T - T_{eq}\right] + \Delta Q$, where κT is the Newtonian relaxation time scale and T_{eq} is the original radiative equilibrium temperature profile. The first perturbation experiment is the BKS run in which ΔQ is added over

Table 1 Numerical model experiments conducted in this study

Experiment name	Description
CTRL	Control run
BKS	An imposed near-surface heating with a seasonal cycle over the BKS region is added to the temperature tendency equation (See Sect. 2 for details)
BKS_ND	Same as BKS run, except that the forcing is only applied in Nov–Dec
BKS_ND_Nudging	Same as BKS_ND run, except that a nudging method is applied to the stratospheric zonal mean state
ESS_ND	Same as BKS_ND run, except that the forcing is located at the Eastern Siberian Sea
ESS_ND_Nudging	Same as BKS_ND_Nudging run, except that the forcing is located at the Eastern Siberian Sea
GLD_ND	Same as BKS_ND run, except that the forcing is located at the Greenland
GLD_ND_Nudging	Same as BKS_ND_Nudging run, except that the forcing is located at the Greenland

the BKS region to mimic the year-to-year variability in near-surface temperature associated with lower than normal BKS SIC. More specifically, $\Delta Q(\lambda, \varphi, \sigma, t)$ is written as follows:

$$AQ = Q_0 \cos^k\left(\frac{1}{4}(\varphi - \varphi_0)\right) e^{m(\sigma-1)} \sin^n\left(\frac{3}{2}\lambda\right) \times \frac{1}{2}\cos\left(\left(t + t_0\right)\frac{2\pi}{365} + 1\right), \quad (1)$$
$$65^\circ \le \varphi, 0^\circ \le \lambda \le 120^\circ E, 1 \le t \le 365,$$

where Q_0 is the maximum heating rate, and parameters k, m, n represent the latitudinal extent, vertical extent and longitudinal extent of the imposed heating, respectively, t is the day number of a year, and λ, φ, and σ denote the longitude, latitude and sigma level in the vertical, respectively. Here we choose $Q_0 = 3.5$ K day^{-1}, $k = 10$, $m = 5$, $n = 2$, $t_0 = 30$ (i.e., maximum heating on Dec 1) and $\varphi_0 = 75^\circ$ to mimic the observed spatial structure and temporal evolution of the near-surface temperature response over the BKS region. Figure 2 shows the horizontal and vertical structures and the temporal evolution of the imposed heating in the BKS experiment. The heating is maximized in Nov–Dec (ND) and decays afterwards following Eq. (1). The resulting maximum equilibrium SAT increase near the forcing center is about 9 K, which is approximately equal to the maximum SAT difference between the low and high Nov BKS SIC index years in the observation. And the results remain similar to varying the heating strength ($Q_0 = 1.5$, 2.0, 2.5, 3.0 and 4.0 K day^{-1}) and other parameters (such as m) of the forcing (to be discussed later).

The second perturbation experiment, namely the BKS_ND run, is the same as the BKS run except that the heating is only applied during ND (see the red curve in Fig. 2c). The third perturbation experiment is the BKS_ND_Nudging run and is similar to the BKS_ND run except that a nudging method is employed in the stratosphere to numerically shut down the stratospheric pathway and thus explicitly isolate the tropospheric pathway (Simpson et al. 2011; Wu and Smith 2016; Nakamura et al. 2016). Specifically, the zonal mean temperature, vorticity and divergence in the stratosphere are nudged towards the reference state from the CTRL experiment at every time step with a nudging coefficient that is 1 above 53 hPa, 0 below 95 hPa and linearly interpolated in between and a nudging time scale of 3-h. With an imposed heating over the BKS region and nudging in the stratosphere, the stratospheric state is not allowed to respond to the forcing because of the nudging, and, consequently, the stratospheric pathway is shut down and the midlatitude circulation response is via the tropospheric pathway only. Wu and Smith (2016) used a similar

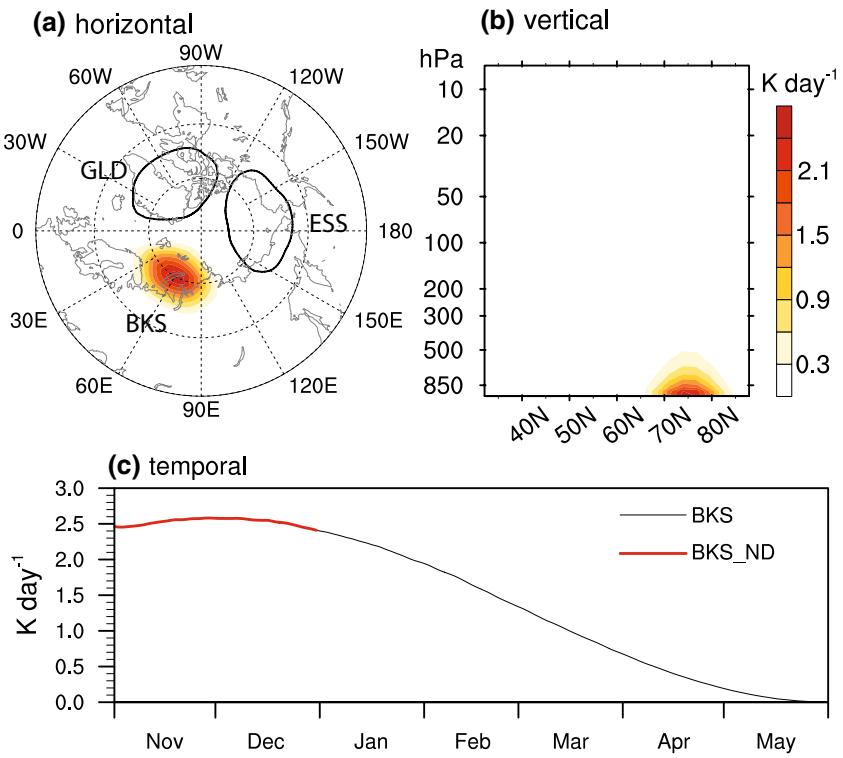

Fig. 2 Imposed Idealized heating (units: K day^{-1}): **a** Horizontal structure, **b** vertical section at 60°E and **c** temporal evolution at the center (60°E, 75°N) at the lowest model level (sigma = 0.947). The *solid black contours* in **a** highlight the forcing location over the East Siberian Sea (ESS) and Greenland (GLD) regions

version of the model but with an imposed warming over the entire Arctic under perpetual winter conditions and they found that the stratospheric pathway is as important as the tropospheric pathway in linking the Arctic amplification with the midlatitude circulation.

In addition, in order to investigate the sensitivity to geographical location of the forcing, we also perform two sets of experiments similar to the BKS_ND run and BKS_ND_Nudging run but with imposed heating shifted by 120° and 240° longitude, more specifically over the East Siberian Sea (ESS_ND run and ESS_ND_Nudging run) and Greenland (GLD_ND run and GLD_ND_Nudging run), respectively. These two forcing locations are highlighted in the Fig. 2a (solid black contours).

The CTRL run is integrated for 140 years and the average of the last 80 years is extracted as the reference state. 80 ensemble runs are conducted for each perturbation experiment with initial conditions taken from the last 80 years of the CTRL. To isolate the effect related to Nov SIC variability (not late summer or early fall SIC variability), the forcing is turned on in the model since Nov 1, and all perturbation experiments integrate from Nov 1 to May 31. The main conclusions of this study are not sensitive to the starting date of the forcing (not shown).

3 Results

3.1 Prolonged effect due to the stratospheric pathway

First of all, we present the circulation response in the idealized model experiments with imposed heating over the BKS region. In the BKS experiment, the polar cap geopotential height (Z_{pcap}), which is obtained from the area-averaged geopotential height over the area north of 67.5°N, increases in the entire troposphere and stratosphere (Fig. 3a), which is qualitatively consistent with previous studies in observations and comprehensive AGCMs (e.g., Kim et al. 2014; Sun et al. 2015). To investigate the prolonged effect as seen in observations (shown in Fig. 1), in the BKS_ND experiment, the near-surface forcing is only imposed during ND and is stopped on Jan 1. Even though the forcing is terminated, the Z_{pcap} response persists in the stratosphere and troposphere for about 40 days until early Feb (Fig. 3b), which is much longer than the typical synoptic time scale in the troposphere. The results remain robust with other choices of forcing parameters and Figure S2 a and c shows an example with a weaker (1.5 K day^{-1}) and a stronger (4.0 K day^{-1}) forcing magnitude and the results are qualitatively similar to Fig. 3b.

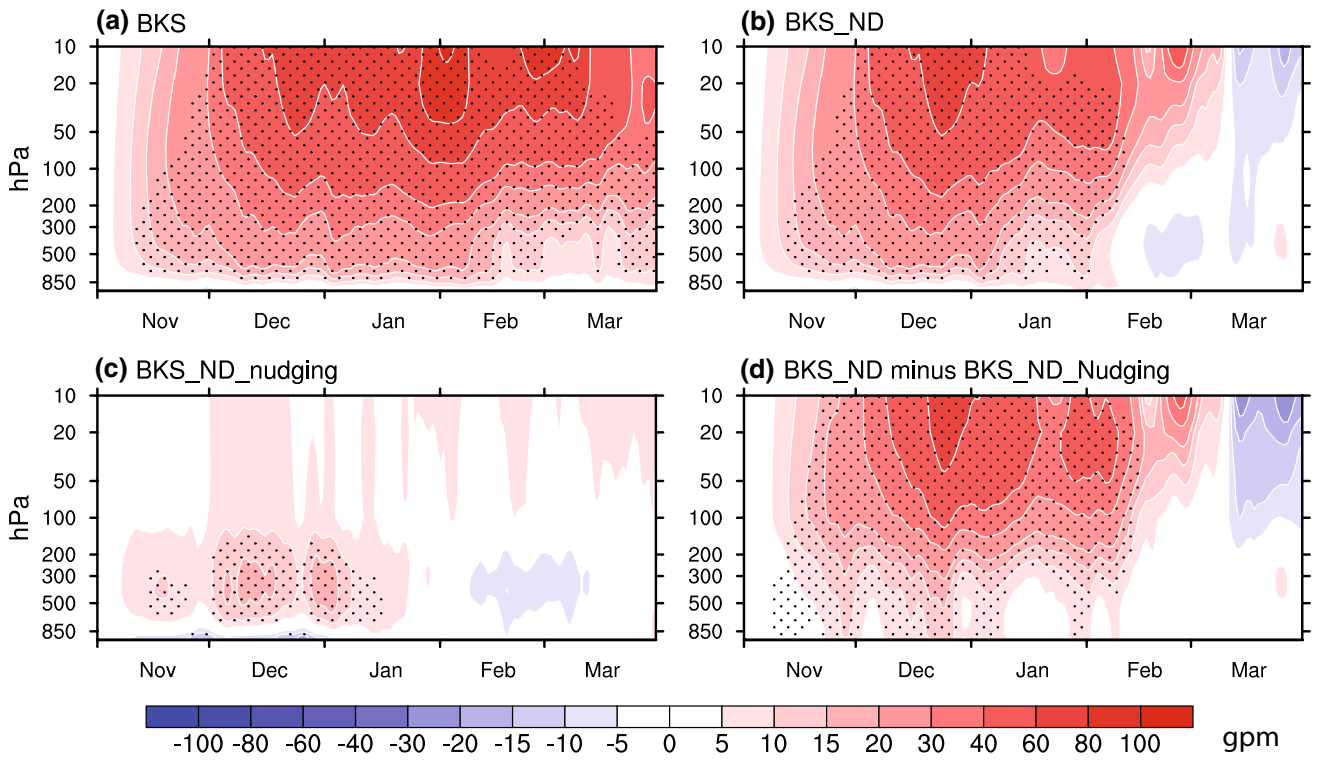

Fig. 3 Time cross sections of the polar cap geopotential height (Z_{pcap}) (units: gpm) response in the BKS (**a**), BKS_ND (**b**) and BKS_ND_Nudging (**c**) experiments. **d** is the difference between the BKS_ND run and the BKS_ND_Nudging run. Stippling denotes the 95% confidence level for the Z_{pcap} response

In the BKS_ND_Nudging experiment, when the stratospheric pathway is removed by the nudging method and only the tropospheric pathway exists, the Z_{pcap} response in the troposphere lasts for only about 15 days (Fig. 3c), which confirms the fact that the enhanced persistence of the response cannot be explained by the tropospheric pathway alone.

A previous study by Wu and Smith (2016) used a similar model version and found that the response via the tropospheric and stratospheric pathway is largely linearly additive, i.e., the sum of the response via the tropospheric and stratospheric pathway can mostly recover the total response. Therefore, here the contribution from the stratospheric pathway can be obtained by the difference of the response in the BKS_ND run and that in the BKS_ND_Nudging run and is shown in Fig. 3d. The evolution of Z_{pcap} in Fig. 3d is similar to that in Fig. 3b and the tropospheric circulation response via the stratospheric pathway can persist until early Feb. This confirms that the stratospheric pathway is an important factor in extending the tropospheric circulation response.

To better quantify the results, we show the response of 700 hPa zonal wind in Fig. 4. The response of 700 hPa zonal wind in Jan in the BKS_ND experiment shows a dipole pattern that deceleration and acceleration are respectively located on the poleward and equatorward sides of the climatological jet axis, which indicates a southward shift of the midlatitude jet (Fig. 4a). The jet response is much weaker when the nudging method is employed in the BKS_ND_Nudging (Fig. 4b). The time evolution of the jet response shows that the jet deceleration in the BKS run is maximized in Feb (black line in Fig. 4c) and the response in the BKS_ND run can persist until early Feb (red line in Fig. 4c), however, the response in the BKS_ND_Nudging experiment is insignificant (blue line in Fig. 4c). More specifically, in Jan, the response in BKS_ND run takes about 70% of the total response in the BKS run, suggesting that 72% of the response in Jan is attributed to ND forcing. Even in Feb, about 44% of the total response in the first 2 weeks of Feb is attributed to ND forcing and the rest is due to the concurrent forcing (not shown). These again demonstrate that the late fall/early winter forcing over the BKS could strongly affect the subsequent winter midlatitude circulation response.

3.2 Dynamical mechanism

The question that is raised here is how the stratospheric pathway works to extend the tropospheric circulation response. We use Eliassen-Palm (EP) flux and 100 hPa eddy heat flux to diagnose wave propagation (e.g., Edmon et al. 1980; Polvani and Waugh 2004; Simpson et al. 2009). In the quasigeostrophic approximation, EP flux is written as $\vec{F} = (F_\varphi, F_P)$, and $F_\varphi = -a\cos\varphi\overline{\langle u * v *\rangle}$ and

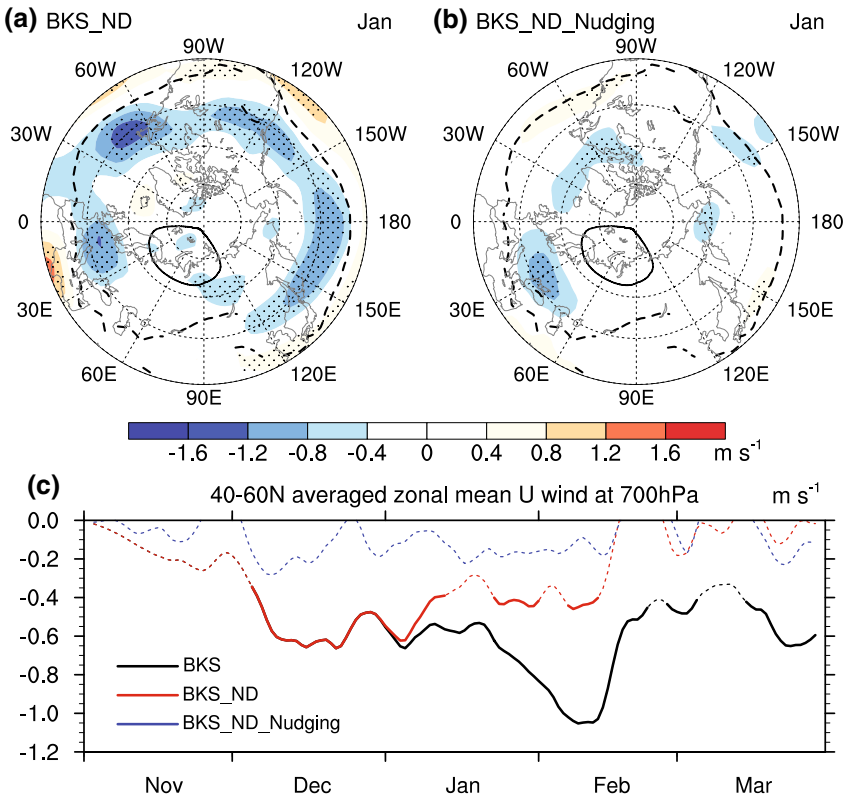

Fig. 4 **a** Responses of 700 hPa zonal wind (units: m s^{-1}) in Jan in the BKS_ND experiment; **b**: same as **a** but for BKS_ND_Nudging; **c**: time series of mid-latitude (40°–60°N) zonal mean zonal wind response (units: m s^{-1}) at 700 hPa in 5-day running mean. The dashed lines in **a** and **b** are the position of westerly jet axis in the control run. Stippling in **a**–**b** denotes the 95% confidence level for zonal wind response. The *solid black contours* in **a**–**b** highlight the forcing location over the BKS region. The *black, red* and *blue lines* in **c** indicate the responses in the BKS, BKS_ND, BKS_ND_Nudging experiments, respectively. The *solid line* segment in **c** highlights the zonal mean zonal wind response that is statistically significant at the 95% confidence level

$F_P = af\cos\varphi\overline{\left\langle \frac{v*\theta*}{\langle\theta\rangle_P}\right\rangle}$, where f is the Coriolis parameter, u and v are zonal and meridional velocities, θ is potential temperature, $\langle\rangle$ denotes zonal average, superscript * denotes deviation from zonal mean and overbar denotes time average. The EP flux divergence is calculated as $\frac{1}{a\cos\varphi}\nabla\cdot\vec{F} = \frac{1}{a\cos\varphi}\left\{\frac{1}{a\cos\varphi}\frac{\partial}{\partial\varphi}(F\varphi\cos\varphi) + \frac{\partial}{\partial P}F_P\right\}$. The direction of EP flux indicates the wave propagation and the flux divergence measures the wave forcing on the zonal wind. In addition, the eddy heat flux anomaly can be decomposed into four components: $\Delta\overline{\langle v*T*\rangle} = \left\langle\Delta\overline{v*}\overline{T}_c^*\right\rangle + \left\langle\Delta\overline{v*}_c\overline{T}^*\right\rangle + \left\langle\Delta\overline{v}^*\overline{T}^*\right\rangle + \Delta\overline{\langle v*'T*'\rangle}$, where Δ is the difference between perturbation experiment and control run, subscript c denotes CTRL run and prime denotes deviation from time average. The first two terms on the right-hand-side are the linear components, the third term is the nonlinear component and the fourth term is the high-frequency fluctuation component.

Here we focus on the BKS_ND experiment. As the Z_{pcap} shown in Fig. 3b and the zonal mean zonal wind in Figure S3 a, as a result of ND near-surface heating, the stratospheric polar vortex weakens in Dec. This circulation response persists in the stratosphere until early Feb accompanied by downward migration back to the troposphere and the surface. We choose Dec as the upward propagation phase, which is before the termination of the forcing (Jan 1). The period of Jan 15–Feb 10 is considered as the downward migration phase, since the tropospheric pathway alone can be ignored about 2 weeks after the termination of the forcing (shown in Fig. 3c), and the delayed response persists for about 40 days until early Feb (as can be seen in Figs. 3b, 4c). This downward migration processes can be better seen by the lead-lag correlation of Z_{pcap} at all levels with Z_{pcap} at 100 hPa in the difference of BKS_ND run and BKS_ND_Nudging run (Figure S4). As can be seen, the signal in the middle-upper stratosphere leads that in the lower stratosphere and troposphere by about 1 week.

During the upward propagation phase, during Dec in the BKS_ND run, anomalous EP flux is excited mostly over 40°–60°N, associated with increased baroclinicity in this region slightly equatorward of the heating anomaly, and planetary-scale waves propagate into the lower stratosphere (Fig. 5a). The EP flux anomaly and its resulting EP flux convergence, which is dominated by its vertical component related to eddy heat flux, is responsible for the weakening of the stratospheric polar vortex (Fig. 5a). The decomposition of the eddy heat flux at 100 hPa shows that this upward propagating wave response can be mainly attributed to its linear component and both the nonlinear and high-frequency components are very small (Fig. 5b). This linear component is due to the linear constructive interference

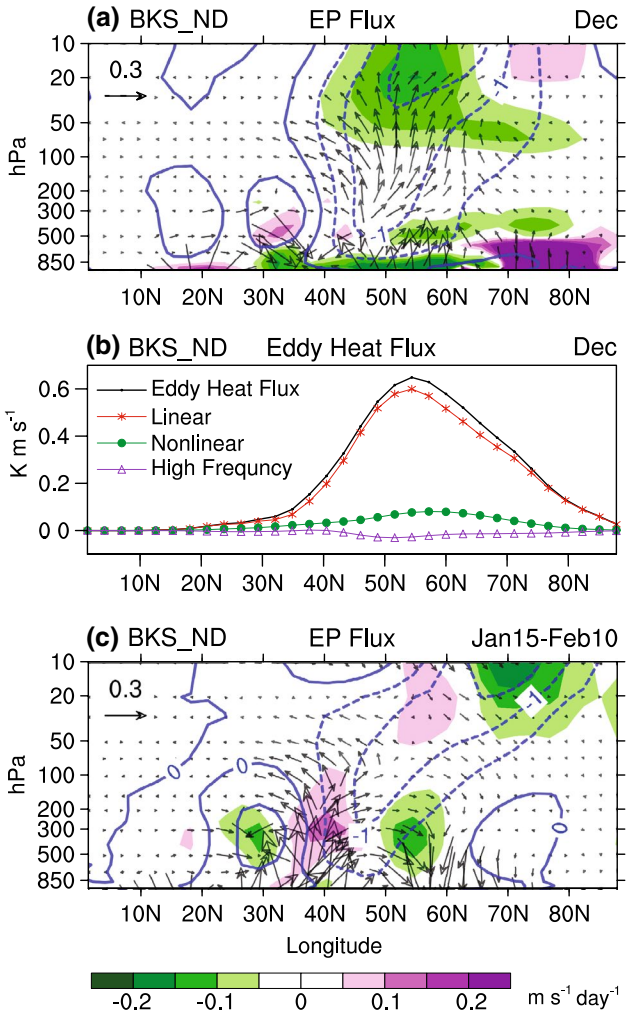

Fig. 5 **a** Response of the EP flux (vector, units: 10^{15} m^3), zonal mean zonal wind (*blue contour*, contour interval is 0.5 m s^{-1} , negative values are *dashed*) and vertical component of the EP flux divergence (*color shading*, units: m s^{-1} day^{-1}) in December in the BK_ND run. The EP flux is multiplied by the square root of 1000/pressure (hPa) to better demonstrate the waves in the stratosphere. **b** Response of 100 hPa zonal mean eddy heat flux (*black*) and its decomposition into linear (*red*), nonlinear (*green*) and high frequency components (*purple*) in December in the BKS_ND run (units: K m s^{-1}). **c** Similar to **a** but during Jan 15–Feb 10 and the *color shading* in **c** is the horizontal component of the EP flux divergence response

mechanism where the wave anomaly is largely in phase with the wave climatology and planetary-scale waves can propagate effectively into the stratosphere [see Fig. 10a and also in Garfinkel et al. (2010) and Smith et al. (2010)].

For the later downward migration phase, during Jan 15–Feb 10, the EP flux response is mostly concentrated in the troposphere (Fig. 5c). Compared to the upward propagation phase, there is anomalous poleward propagating EP flux in the midlatitude troposphere, indicating the critical role of eddy momentum flux. The convergence of anomalous EP flux, dominated by eddy momentum flux

component, at about 40°–60°N favors the persistence of the midlatitude westerly deceleration in the troposphere. The detailed mechanism of downward migration has been examined extensively in previous studies (e.g., Hartley et al. 1998; Perlwitz and Harnik 2003; Kushner and Polvani 2004; Song and Robinson 2004; Simpson et al. 2009) and is beyond the scope of this study.

3.3 Induced cold winter over central Asia

In addition to the midlatitude jet response, another consequence of Arctic sea ice melting is its possible impact on Eurasian cold air outbreaks, but the evidence for this impact is less clear. Some studies attribute the increased mid-latitude extremes in recent years to the declining trend of Arctic sea ice (e.g., Honda et al. 2009; Petoukhov and Semenov 2010; Francis and Vavrus 2012; Cohen et al. 2014; Mori et al. 2014; Kug et al. 2015); however, others argue that there is no robust response or, in contrast, fewer extremes to Arctic sea ice loss (Barnes 2013; Hassanzadeh et al. 2014; Li et al. 2015; McCusker et al. 2016; Sellevold et al. 2016; Sun et al. 2016). Here, we simply document the results from our idealized AGCM experiments. Figure 6 shows the circulation and temperature response in Dec in the BKS_ND run and BKS_ND_Nudging run. As shown in Fig. 6b, there is an induced cold response over central Asia as a result of imposed heating over the BKS region, which resembles that in observations (shown in Fig. 1a). This induced cold anomaly remains robust with other choices of forcing parameters (see Figure S2 b and d for an example with a weaker (1.5 K day^{-1}) and a stronger (4.0 K day^{-1}) forcing magnitude). This cold response is also deep in the vertical column in troposphere (Fig. 6a). However, this cold response becomes weaker in the nudging experiment in which the stratospheric pathway is deactivated (Fig. 6b, d), and this demonstrates that the stratospheric pathway also plays an important role in amplifying the central Asia cold events. Figure 7 is similar to Fig. 6 but for Jan. Even though the forcing is switched off, a cold response can still be seen over central Asia in the BKS_ND experiment. However,

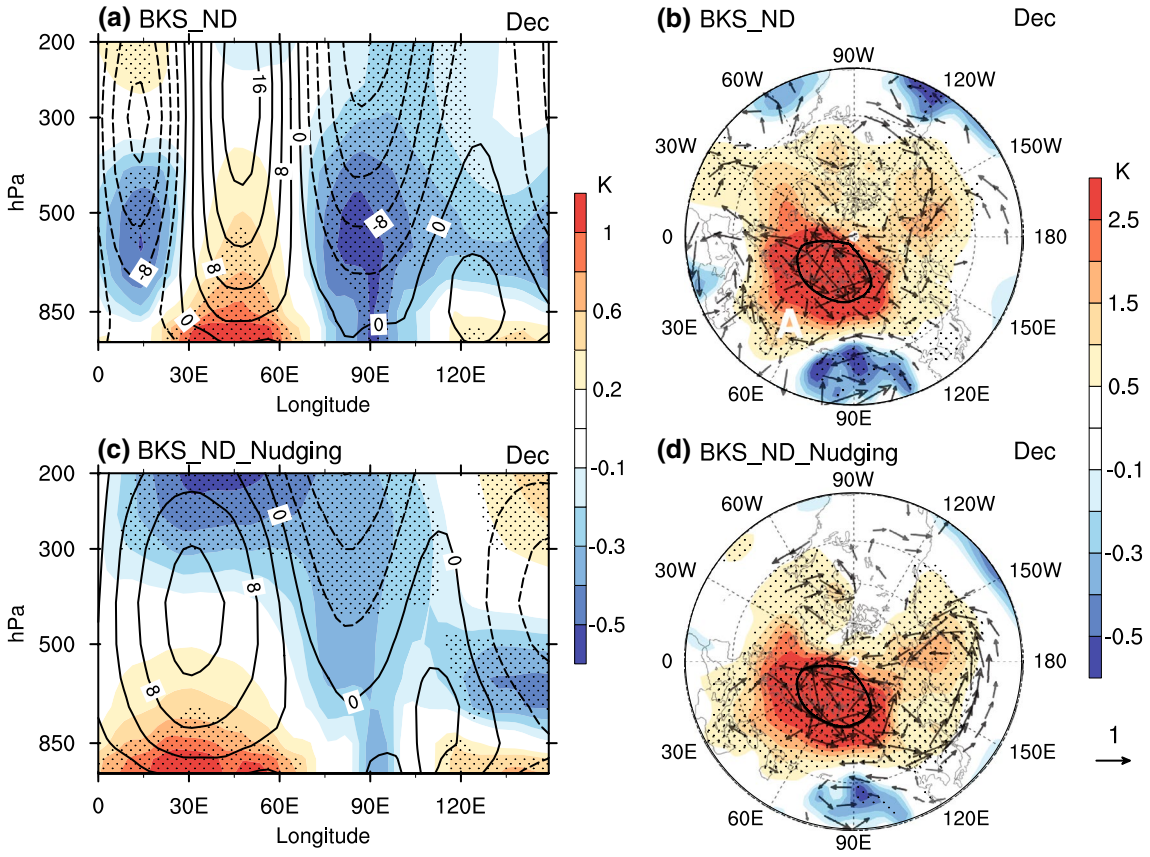

Fig. 6 **a** 40°–50°N averaged longitude-pressure cross-section of temperature (*color shading*) and geopotential height (*contour*, contour interval is 4 gpm, negative values are *dashed*) responses in December in the BKS_ND run. **b** Response of temperature (*color shading*, units: K) and wind (vector, units: m s^{-1}) at the lowest model level (sigma = 0.947) in January in the BKS_ND run. **c** and **d** Same as **a** and **b** but for the BKS_ND_Nudging experiment. The *white symbol 'A'* in **b** highlights the anticyclonic anomalies. Stippling denotes the 95% confidence level for temperature. Only the surface wind response at the 95% confidence level is shown in **b** and **d**. The *solid black contour* in **b, d** highlights the forcing location

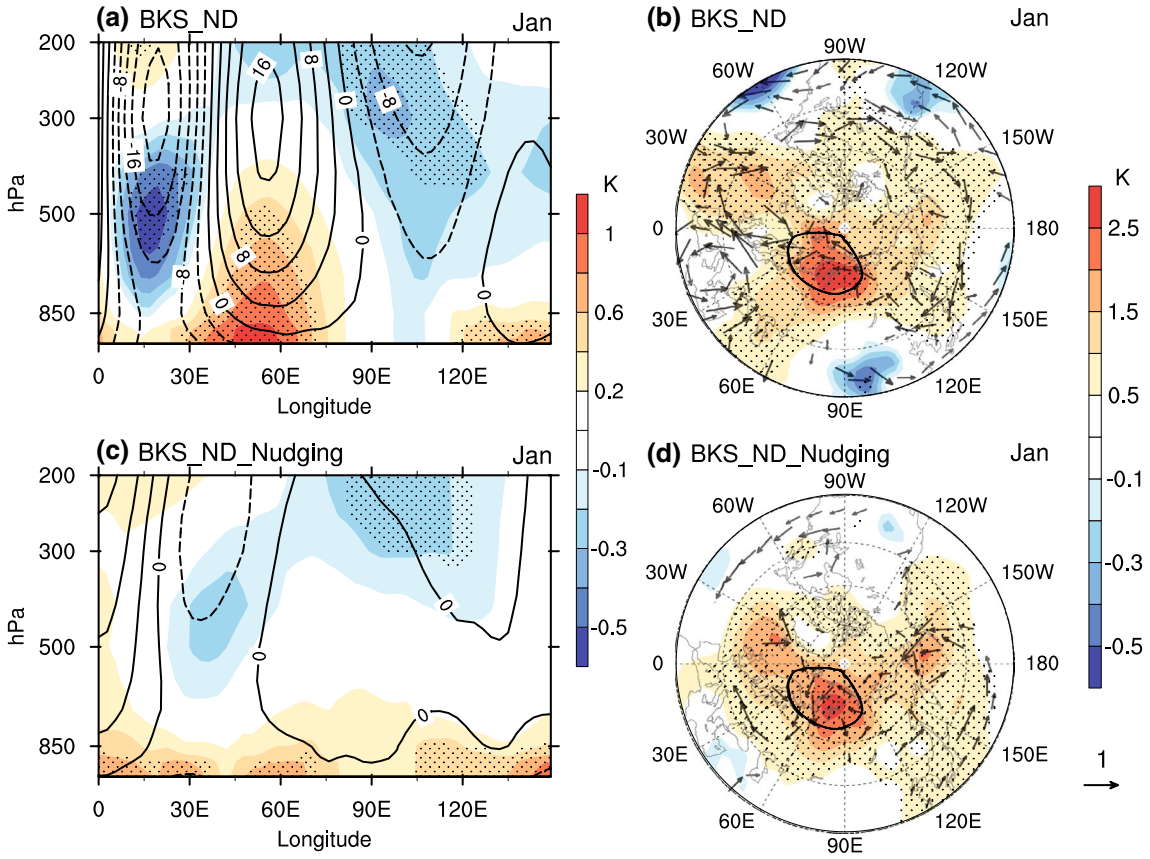

Fig. 7 Same as Fig. 6 but for January

the cold response almost disappears near the surface in the BKS_ND_Nudging experiment and the lower stratosphere upper troposphere and the surface appears de-coupled.

This induced cold anomaly over central Asia is mainly a result of the circulation response. A negative Arctic Oscillation (AO)-like pattern is found over the NH extra-tropics (figure not shown) and an anomalous deep warm high ridge is found near the Ural Mountains (35°–65°E) and occupies the entire troposphere (Fig. 6a), which is in agreement with observations and comprehensive model experiments (e.g., Mori et al. 2014; Cohen et al. 2014; Overland et al. 2015). The accompanied anticyclonic circulation anomaly, even though weak in magnitude, is found on the southern side of BKS forcing (highlighted by the white symbol 'A' in Fig. 6b), which is consistent with observations and comprehensive model experiments (see Fig. 1 in Mori et al. 2014). The high ridge near the Ural Mountains and the associated northerly wind to the east leads to more cold air advection from the Arctic region to central Asia (Fig. 6b). The high ridge and the northerly flow are weaker in the nudging experiment (Fig. 6c, d), which is responsible for the weaker cold anomaly over central Asia. Similar circulation response can be seen in Jan (Fig. 7). These results suggest that the existence of the stratospheric pathway, i.e., the dynamical coupling between the troposphere and stratosphere, acts to enhance the intensity and prolong the duration of midlatitude ridge/trough, resulting in enhanced surface cooling response over central Asia.

3.4 Sensitivity to geographical location of the forcing

Recent studies suggested that the sea ice loss in different regions over the Arctic might have different impacts on the midlatitude circulation (Sun et al. 2015; Koenigk et al. 2016; Pedersen et al. 2016). Therefore, in addition to the BKS experiments, here we also investigate the sensitivity of the midlatitude circulation response to geographical location of the forcing, more specifically over the East Siberian Sea (ESS) and Greenland (GLD) (see Fig. 2a), by using the idealized model.

Figure 8a is similar to Fig. 3b but for the ESS_ND experiments, in which the forcing is imposed during ND over the ESS region. The Z_{pcap} also increases in the troposphere and lower stratosphere but the intensity is weaker, especially in the stratosphere, and the persistence is shorter than that in the BKS_ND run. In the nudging experiment

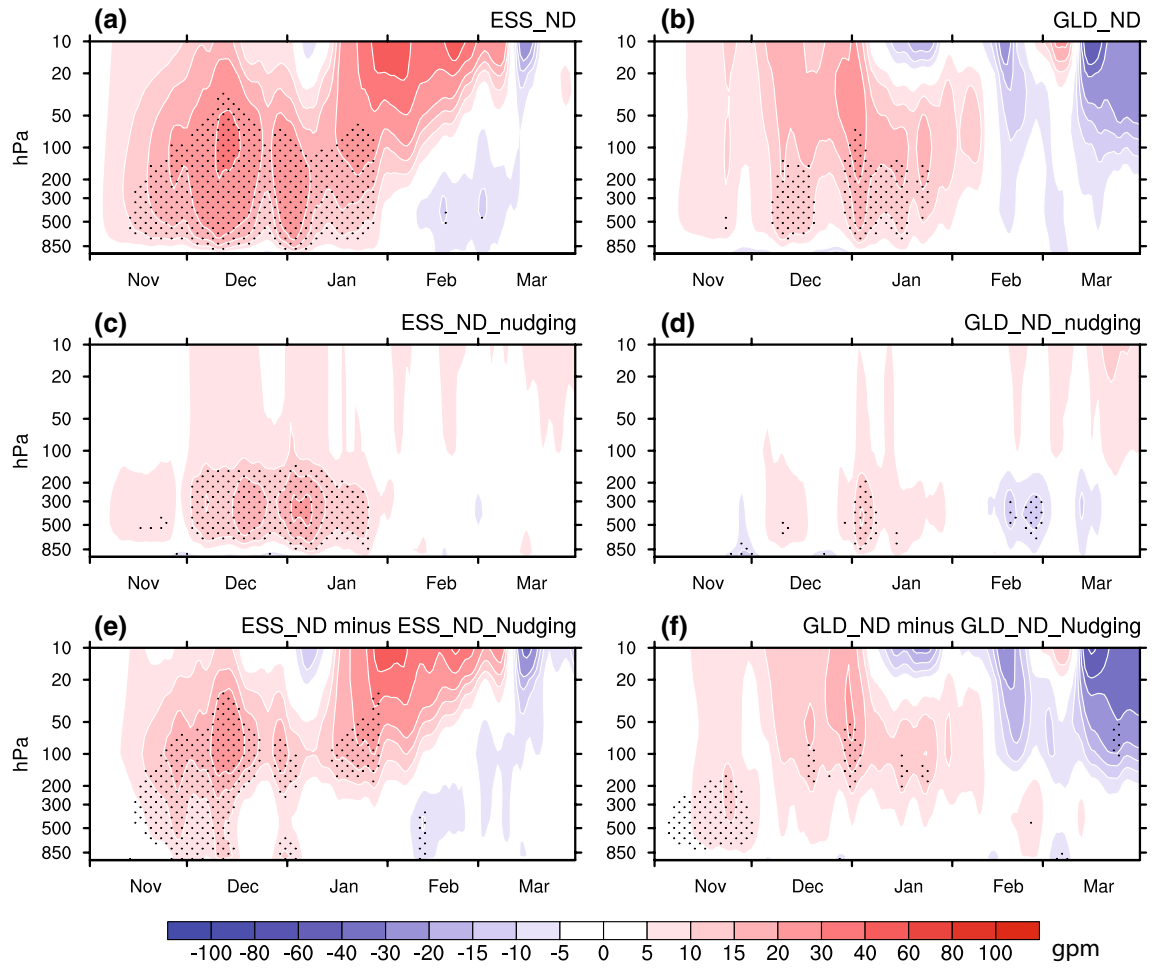

Fig. 8 **a, c** and **e** same as Fig. 3b–d but for forcing centered at East Siberian Sea (ESS); **b, d** and **f** same as Fig. 3b–d but for forcing centered at Greenland (GLD)

for ESS_ND forcing (Fig. 8c), the tropospheric pathway is comparable to that in BKS_ND forcing experiment. However, the stratospheric response and downward migration is nearly absent after the termination of the forcing (Fig. 8e). In the GLD_ND experiment, the Z_{pcap} response is very weak both in the troposphere and stratosphere (Fig. 8b) with both weak tropospheric and stratospheric pathways (Fig. 8d, f).

Figure 9 compares the midlatitude low-level jet response in the BKS_ND, ESS_ND and GLD_ND experiments. In the ESS_ND run, the midlatitude low-level jet response is comparable to that in the BKS_ND run in Dec, but is not robust beyond early Jan. The ESS_ND forcing induced circulation is mostly due to the tropospheric adjustment itself with a minor contribution from stratosphere-troposphere coupling (Figure S5). The lack of prolonged stratospheric downward migration effect by the ESS_ND forcing likely contributes to the short persistence of the tropospheric jet response. The jet response in GLD_ND run is very weak

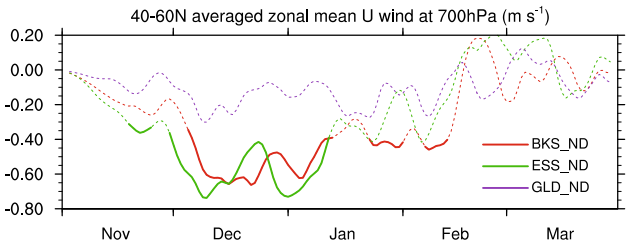

Fig. 9 Same as Fig. 4c but for ESS_ND run (*green*) and GLD_ND run (*purple*). The *red line* is BKS_ND run, same as the *red line* in Fig. 4c

and is insignificant, which is due to the weak response via both the tropospheric and stratospheric pathway.

Compared to the BKS_ND run, although the structure and intensity of the forcing is exactly same in the ESS_ND run and GLD_ND run, the circulation responses are different in those experiments, which imply that the midlatitude

response and troposphere–stratosphere coupling are sensitive to the geographical location of the forcing.

To better understand the stratosphere–troposphere coupling to geographical location for the forcing, Fig. 10 shows the response of zonal wave-1 and wave-2 geopotential height. It is found that the BKS region is close to the climatological ridge of both wave-1 and wave-2 and thus the BKS forcing excites anomalous ridge in phase with the climatology. This planetary wave response in-phase with the control state is known as linear constructive interference and effectively excites the vertical wave propagation into stratosphere and a weaker polar vortex (see Sect. 3.2 Smith et al. 2010). The BKS_ND forcing induced wave-1 and wave-2 responses are consistent with previous observation and comprehensive model results (e.g., Kim et al. 2014; Mori et al. 2014; Sun et al. 2015). On the contrary, the excited wave-1 and wave-2 anomalies in ESS_ND (Fig. 10b, e) and wave-1 anomalies in GLD_ND experiments (Fig. 10c) are mostly out-of-phase with the control state. Although the wave-2 anomalies in GLD_ND experiment are in-phase with the control state (Fig. 10f), its contribution is much smaller than that of the wave-1 and thus the total response in GLD_ND experiment is still linear deconstructive. This linear deconstructive interference in the troposphere-stratosphere coupling leads to a slightly enhanced polar vortex over high latitudes (Figure S3b, c). In view of Z_{pcap}, it should be noted that the geopotential height is a vertically-integrated quantity and therefore,

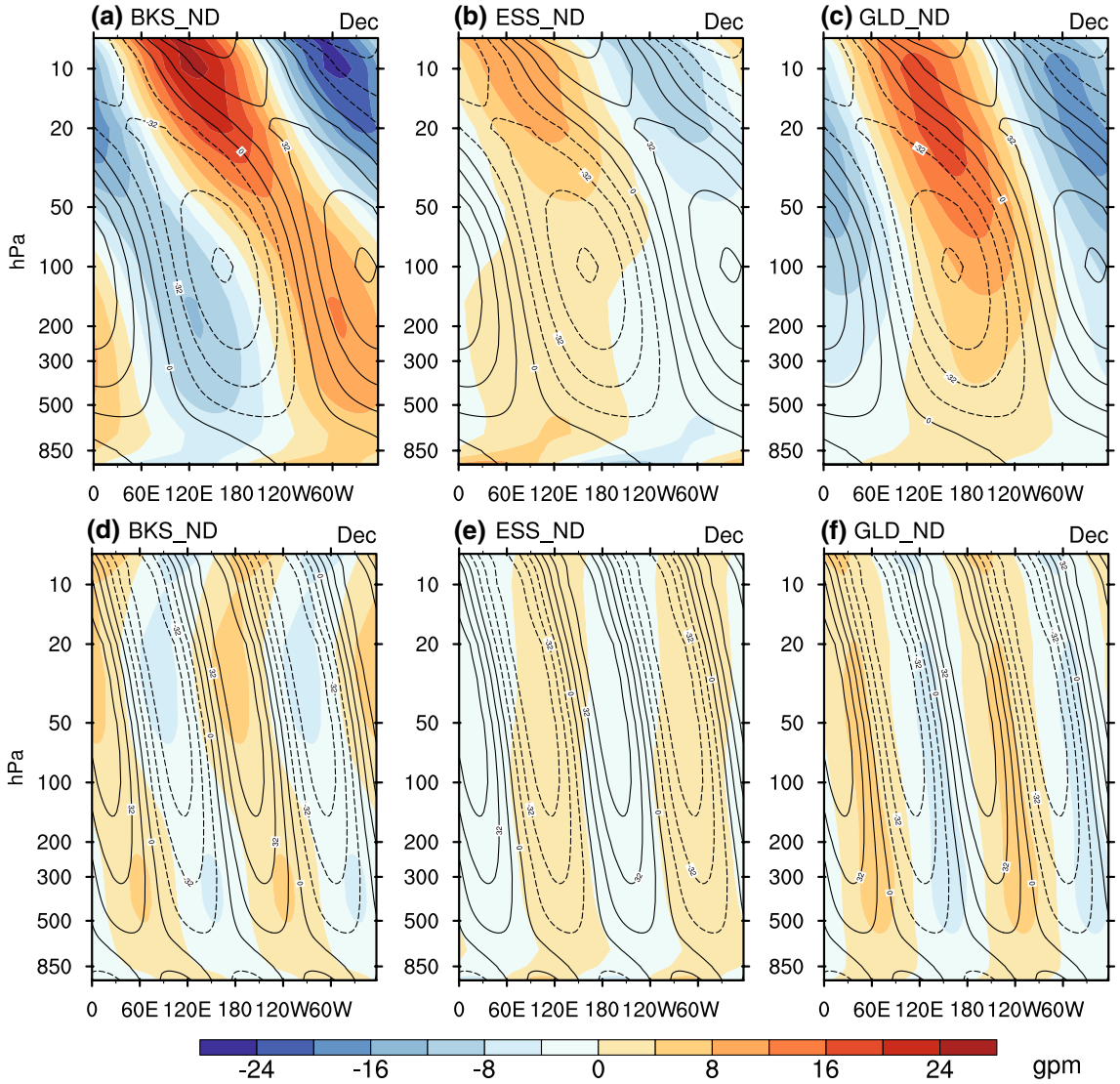

Fig. 10 45°–70°N averaged zonal wave-1 geopotential height (units: gpm, contour interval is 16 gpm) in the control run (contour, negative *dashed*), wave-1 response in the BKS_ND run (**a**), ESS_ND run (**b**) and GLD_ND run (**c**) (*color shading*) and wave-2 response in the BKS_ND run (**d**), ESS_ND run (**e**) and GLD_ND run (**f**) (*color shading*) in Dec

surface anomalies due to the imposed heating could affect the upper levels. However, the dynamical linear deconstructive interference acts in an opposite manner, partly offsets the Z_{pcap} increase due to the surface temperature increase and leads to weaker Z_{pcap} responses in those two experiments compared to that in BKS_ND run (Fig. 8). Thus, the resulting weaker responses via the stratospheric pathway in ESS_ND and GLD_ND experiments account for the short-lived and weaker responses in the midlatitude circulation (Figs. 8, 9). These results suggest that the BKS region is the most effective in influencing the midlatitude circulation through more active stratospheric pathway than other regions over the Arctic.

4 Conclusion and discussion

In this study we investigate the observed lead-lag correlation between the early winter BKS sea ice variability and the later winter midlatitude circulation response using a set of idealized AGCM experiments. First of all, the experiment results show that the idealized dry model is able to reproduce the persistent winter circulation response during Jan–Feb with an imposed near-surface heating during Nov–Dec. Then by applying a nudging method in the stratosphere and an explicit separation of the tropospheric and stratospheric pathway, it is found that the prolonged midlatitude circulation response is largely due to the stratospheric pathway and the long time scale in the stratosphere. Second, the dynamic diagnostic results show that the stratospheric pathway works in two phases: the first phase involves upward propagation of planetary-scale waves due to linear constructive interference and the weakening of the stratospheric polar vortex; the second phase involves downward migration from the stratosphere to the troposphere and the surface. This downward migration largely amplifies and extends the low-level jet deceleration. Third, as a result of the imposed heating over the BKS region, an induced cold anomaly is simulated over central Asia, which resembles the feature seen in observations. It is found that the stratospheric pathway also acts to amplify and extend the cold events over central Asia. Above results qualitatively remain robust when varying the forcing parameters. Finally, further experiments show that the midlatitude circulation response is sensitive to the geographical location of the forcing. The BKS region is found the most effective in influencing the midlatitude circulation response than other regions over the Arctic.

The results found in this idealized model setup are largely in agreement with previous studies that suggest an important role of the stratospheric pathway in linking the Arctic sea ice with the midlatitude circulation (e.g., Kim et al. 2014; Sun et al. 2015; Nakamura et al. 2016; Yang et al. 2016). In contrast with similar studies, we explicitly separate the tropospheric and stratospheric pathway and unequivocally attribute the prolonged midlatitude circulation response to the stratospheric pathway and its long time scale. We plan to extend our work to state-of-the-art AGCM and realistic variability of Arctic sea ice to better quantify the lead-lag effect and the role of the stratospheric pathway in future study. This prolonged effect of the stratospheric pathway may be helpful in better understanding and predicting the midlatitude winter conditions (Scaife et al. 2014).

Acknowledgements The authors thank Dr. Linjiong Zhou at GFDL for model stability testing and Dr. Yueyue Yu at Florida State University for discussion. PZ and YW are supported by the U.S. National Science Foundation (NSF) Climate and Large-Scale Dynamics program under Grant AGS-1406962 and a start-up fund from the Department of Earth, Atmospheric, and Planetary Sciences at Purdue University. KLS is funded by the NSF Office of Polar Programs, Arctic Research Opportunities, PLR-1603350.

References

Baldwin MP, Stephenson DB, Thompson DWJ, Dunkerton TJ, Charlton AJ, O'Neill A (2003) Stratospheric memory and skill of extended-range weather forecasts. Science 301:636–640. doi:10.1126/science.1087143

Barnes EA (2013) Revisiting the evidence linking Arctic amplification to extreme weather in midlatitudes. Geophys Res Lett 40(17):4734–4739. doi:10.1002/grl.50880

Barnes EA, Screen JA (2015) The impact of Arctic warming on the midlatitude jet-stream: Can it? Has it? Will it? Wiley Interdiscip Rev Clim Change 6(3):277–286. doi:10.1002/wcc.337

Butler A, Thompson D, Heikes R (2010) The steady-state atmospheric circulation response to climate change–like thermal forcings in a simple general circulation model. J Clim 23:3474–3496

Cavalieri DJ, Parkinson CL, Gloersen P, Zwally HJ (1996) Sea ice concentrations from Nimbus-7 SMMR and DMSP SSM/I-SSMIS passive microwave data. National Snow and Ice Data Center. Boulder

Cohen J., Screen JA, Furtado JC et al (2014) Recent Arctic amplification and extreme mid-latitude weather. Nat Geosci 7(9):627–637. doi:10.1038/ngeo2234

Dee DP et al (2011) The ERA-Interim reanalysis: configuration and performance of the data assimilation system. Q J R Meteorolog Soc 137(656):553–597. doi:10.1002/qj.828

Deser C, Magnusdottir G, Saravanan R, Phillips A (2004) The Effects of North Atlantic SST and sea ice anomalies on the winter circulation in CCM3. Part II: direct and indirect components of the response. J Clim 17(5):877–889. doi:10.1175/1520-0442(2004)017<0877:TEONAS>2.0.CO;2

Edmon HJ, Hoskins BJ, McIntyre ME (1980) Eliassen-Palm cross sections for the troposphere. J Atmos Sci 37(12):2600–2616. doi:10.1175/1520-0469(1980)037<2600:EPCSFT>2.0.CO;2

Francis JA, Vavrus SJ (2012) Evidence linking Arctic amplification to extreme weather in mid-latitudes. Geophys Res Lett 39(6):L06801. doi:10.1029/2012GL051000

Garfinkel CI, Hartmann DL, Sassi F (2010) Tropospheric precursors of anomalous northern hemisphere stratospheric polar vortices. J Clim 23(12):3282–3299. doi:10.1175/2010JCLI3010.1

Hartley DE, Villarin JT, Black RX, Davis CA (1998) A new perspective on the dynamical link between the stratosphere and troposphere. Nature 391(6666):471–474

Hassanzadeh P, Kuang Z (2015) Blocking variability: Arctic amplification versus Arctic oscillation. Geophys Res Lett. doi:10.1002/2015GL065923**(2015GL065923)**

Hassanzadeh P, Kuang Z, Farrell BF (2014) Responses of midlatitude blocks and wave amplitude to changes in the meridional temperature gradient in an idealized dry GCM. Geophys Res Lett 41(14):5223–5232. doi:10.1002/2014GL060764

Held IM, Suarez MJ (1994) A proposal for the intercomparison of the dynamical cores of atmospheric general circulation models. Bull Am Meteorol Soc 75(10):1825–1830. doi:10.1175/1520-0477(1994)075<1825:APFTIO>2.0.CO;2

Honda M, Inoue J, Yamane S (2009) Influence of low Arctic sea ice minima on anomalously cold Eurasian winters. Geophys Res Lett 36(8):L08707. doi:10.1029/2008GL037079

Jaiser R, Dethloff K, Handorf D (2013) Stratospheric response to Arctic sea ice retreat and associated planetary wave propagation changes. Tellus A 65:19375. doi:10.3402/tellusa.v65i0.19375

Kim B-M, Son S-W, Min S-K, Jeong J-H, Kim S-J, Zhang X, Shim T, Yoon J-H (2014) Weakening of the stratospheric polar vortex by Arctic sea-ice loss. Nat Commun. doi:10.1038/ncomms5646

Koenigk T, Caian M, Nikulin G, Schimanke S (2016) Regional Arctic sea ice variations as predictor for winter climate conditions. Clim Dynam 46(1):317–337. doi:10.1007/s00382-015-2586-1

Kug J-S, Jeong J-H, Jang Y-S, Kim B-M, Folland C K, Min S-K, Son S-W (2015) Two distinct influences of Arctic warming on cold winters over North America and East Asia. Nat Geosci 8(10):759–762. doi:10.1038/ngeo2517

Kushner PJ, Polvani LM (2004) Stratosphere–troposphere coupling in a relatively simple AGCM: the role of eddies. J Clim 17(3):629–639

Kushner PJ, Polvani LM (2006) Stratosphere–troposphere coupling in a relatively simple AGCM: impact of the seasonal cycle. J Clim 19(21):5721–5727. doi:10.1175/JCLI4007.1

Lee M-Y, Hong C-C, Hsu H-H (2015) Compounding effects of warm sea surface temperature and reduced sea ice on the extreme circulation over the extratropical North Pacific and North America during the 2013–2014 boreal winter. Geophys Res Lett 42(5):2014GL062956. doi:10.1002/2014GL062956

Li C, Stevens B, Marotzke J (2015) Eurasian winter cooling in the warming hiatus of 1998–2012. Geophys Res Lett 42(19):2015GL065327. doi:10.1002/2015GL065327

McCusker KE, Fyfe JC, Sigmond M (2016) Twenty-five winters of unexpected Eurasian cooling unlikely due to Arctic sea-ice loss. Nature Geosci 9(11):838–842

Mori M, Watanabe M, Shiogama H, Inoue J, Kimoto M (2014) Robust Arctic sea-ice influence on the frequent Eurasian cold winters in past decades. Nat Geosci 7(12):869–873. doi:10.1038/ngeo2277

Nakamura T, Yamazaki K, Iwamoto K, Honda M, Miyoshi Y, Ogawa Y, Tomikawa Y, Ukita J (2016) The stratospheric pathway for Arctic impacts on midlatitude climate. Geophys Res Lett. doi:10.1002/2016GL068330**(2016GL068330)**

Overland J, Francis JA, Hall R, Hanna E, Kim S-J, Vihma T (2015) The melting Arctic and midlatitude Weather patterns: are they connected? J Clim 28(20):7917–7932. doi:10.1175/JCLI-D-14-00822.1

Pedersen RA, Cvijanovic I, Langen PL, Vinther BM (2016) The impact of regional Arctic Sea ice loss on atmospheric circulation and the NAO. J Clim 29:889–902

Perlwitz J, Harnik N (2003) Observational evidence of a stratospheric influence on the troposphere by planetary wave reflection. J Clim 16:3011–3026

Petoukhov V, Semenov VA (2010) A link between reduced Barents–Kara sea ice and cold winter extremes over northern continents. J Geophys Res Atmos 115(D21):D21111. doi:10.1029/2009JD013568

Polvani LM, Kushner PJ (2002) Tropospheric response to stratospheric perturbations in a relatively simple general circulation model. Geophys Res Lett 29(7):18-11-18-14. doi:10.1029/2001GL014284

Polvani LM, Waugh DW (2004) Upward wave activity flux as a precursor to extreme stratospheric events and subsequent anomalous surface weather regimes. J Clim 17(18):3548–3554. doi:10.1175/1520-0442(2004)017<3548:UWAFAA>2.0.CO;2

Reynolds RW, Rayner NA, Smith TM, Stokes DC, Wang W (2002) An improved in situ and satellite SST analysis for climate. J Clim 15(13):1609–1625. doi:10.1175/1520-0442(2002)015<1609:AIISAS>2.0.CO;2

Scaife AA et al (2014) Skillful long-range prediction of European and North American winters. Geophys Res Lett 41(7):2014GL059637. doi:10.1002/2014GL059637

Screen AJ, Deser C, Sun L (2015) Projected changes in regional climate extremes arising from Arctic sea ice loss. Environ Res Lett 10(8):084006

Sellevold R, Sobolowski S, Li C (2016) Investigating possible Arctic–midlatitude teleconnections in a linear framework. J Clim 29(20):7329–7343

Simpson IR, Blackburn M, Haigh JD (2009) The role of eddies in driving the tropospheric response to stratospheric heating perturbations. J Atmos Sci 66(5):1347–1365. doi:10.1175/2008JAS2758.1

Simpson IR, Hitchcock P, Shepherd TG, Scinocca JF (2011) Stratospheric variability and tropospheric annular-mode timescales. Geophys Res Lett 38(20):L20806. doi:10.1029/2011GL049304

Smith KL, Fletche CG, Kushner PJ (2010) The role of linear interference in the annular mode response to extratropical surface forcing. J Clim 23(22):6036–6050. doi:10.1175/2010JCLI3606.1

Song Y, Robinsion W (2004) Dynamical mechanisms for stratospheric influences on the troposphere. J Atmos Sci 61(14):1711–1725

Sun L, Deser C, Tomas RA (2015) Mechanisms of stratospheric and tropospheric circulation response to projected arctic sea ice loss. J Clim 28(19):7824–7845. doi:10.1175/JCLI-D-15-0169.1

Sun L, Perlwitz J, Hoerling M (2016) What caused the recent "Warm Arctic, Cold Continents" trend pattern in winter temperatures? Geophys Res Lett. doi:10.1002/2016GL069024**(2016GL069024)**

Vihma T (2014) Effects of Arctic sea ice decline on weather and climate: a review. Surv Geophys 35(5):1175–1214. doi:10.1007/s10712-014-9284-0

Wu Y, Smith KL (2016) Response of northern hemisphere midlatitude circulation to arctic amplification in a simple atmospheric general circulation model. J Clim. doi:10.1175/JCLI-D-15-0602.1

Wu Q, Zhang X (2010) Observed forcing-feedback processes between Northern Hemisphere atmospheric circulation and Arctic sea ice coverage. J Geophys Res Atmos 115(D14):D14119. doi:10.1029/2009JD013574

Yang X-Y, Yuan X, Ting M (2016) Dynamical link between the Barents–Kara Sea ice and the Arctic oscillation. J Clim 29:5103–5122. doi: 10.1175/JCLI-D-15-0669.1